describes the effect of the slot discontinuity, i.e., the coupling of the eigenmodes of the undisturbed structure. The eigenvalues, i.e., the resonance frequencies of the resonator are found if the eigenvalue equation

$$\det(\overleftrightarrow{S}\cdot\overleftrightarrow{P}+\overleftrightarrow{S'})=0 \qquad \text{(A.13)}$$

is satisfied, that means if the zeros of the system determinant are found.

References

[1] R. M. Knox, "Dielectric waveguide microwave integrated circuits—an overview," *IEEE Trans. Microwave Theory Tech.*, vol. MTT-24, Nov. 1976, pp. 806–814.

[2] T. Itoh and F.-J. Hsu, "Distributed bragg reflector gunn oscillators for dielectric millimeter-wave integrated circuits," *IEEE Trans. Microwave Theory Tech.*, vol. MTT-27, May 1979, pp. 514–518.

[3] K. Solbach, "Grating-tuner in dielectric image line for integrated millimeterwave circuits," *Dig. 9th European Microwave Conf.*, (Brighton, England), pp. 458–462, Sept. 1979.

[4] W. K. McRitchie and J. C. Beal, "Yagi-Uda array as a surface-wave launcher for dielectric image lines," *IEEE Trans. Microwave Theory Tech.*, vol. MTT-20, Aug. 1972, pp. 493–496.

[5] J. Galejs, "Driving point impedance of linear antennas in the presence of a stratified dielectric," *IEEE Trans. Antennas Propagat.*, vol. AP-13, Sept. 1965, pp. 725–736.

[6] R. H. Duhamel and J. W. Duncan, "Launching efficiency of wires and slots for dielectric rod waveguide," *IRE Trans. Microwave Theory Tech.*, vol. MTT-6, Mar. 1958, pp. 277–284.

[7] R. F. Harrington, *Time-harmonic electromagnetic fields*. New York: McGraw-Hill, 1961.

Propagation Properties of a Planar Dielectric Waveguide with Periodic Metallic Strips

KAZUHIKO OGUSU, MEMBER, IEEE

***Abstract*—A dielectric waveguide with periodic metallic strips suitable for millimeter-wave and submillimeter-wave integrated circuits is analyzed by a rigorous formulation. The accuracy of the solution of our analysis can be systematically improved by increasing the size of the matrix associated with the eigenvalue equation. Stopband properties are numerically presented as a function of the spacing and width of metallic strips and dielectric profile. It is found that there is a difference in the stopband properties of TM and TE modes. Experimental results for the band reject filter are also presented to verify the validity of our analysis.**

I. Introduction

DIELECTRIC periodic structures have been applied to many devices in integrated optics, such as filters [1], [2], input and output beam couplers [3], [4], and distributed feedback lasers [5]. At millimeter and submillimeter wavelengths too, they can be applied to devices similar to those in integrated optics. Although a few investigations have been reported [6], periodic structures have not yet been widely used in millimeter-wave and submillimeter-wave integrated circuits.

The purpose of the present paper is to determine the propagation properties of a planar dielectric waveguide with periodic metallic strips as shown in Fig. 1. This periodic structure can be easily and accurately fabricated by existing printed-circuit techniques for microstrip microwave integrated circuits and is suitable for millimeter-wave and submillimeter-wave integrated circuits. The propagation properties are characterized by the film thickness, width and spacing of metallic strips, dielectric profile, and operating frequency. We restrict the discussion to the stopband phenomenon applicable to band reject filters, since the scattering properties of similar periodic structures with metallic strips are discussed in several articles and texts [7]–[9]. The theoretical analysis is essentially the same as the spectral domain approach [10], [11], which is a powerful tool for the analysis of striplines.

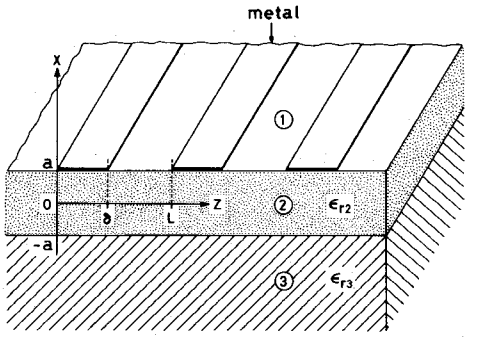

Fig. 1. Geometry of the dielectric waveguide with periodic metallic strips. Regions 1, 2, and 3 correspond to a cover (air), guiding film, and substrate, respectively.

The width and center frequency of the stopband and attenuation constant at the center frequency are numerically presented as a function of the width and spacing of the metallic strips and dielectric profile. It is found that there is a difference in the stopband properties of TM and

Manuscript received December 6, 1979; revised August 27, 1980.

The author is with the Faculty of Engineering, Shizuoka University, Hamamatsu, 432 Japan.

0018-9480/81/0100-0016$00.75 ©1981 IEEE

TE modes. The results of an experiment confirming the theoretical results are also presented.

II. Formulation of the Problem

Fig. 1 shows the geometry of the planar dielectric waveguide with periodic metallic strips and the coordinate system for the present analysis. Regions 1, 2, and 3 correspond to a cover, guiding film, and substrate, respectively. In our case, the cover material is air. The metallic strips are placed on the top of the film at periodic intervals L. We assume that the metal and dielectric materials are lossless. Since both TM and TE modes can be analyzed in a similar manner, we will consider only the TM modes with no variation in the y direction.

The TM modes have three nonvanishing field components; H_y, E_x, and E_z. The E_x and E_z components are represented in terms of the H_y component as

$$E_x = \frac{j}{\omega\epsilon_r\epsilon_0}\frac{\partial H_y}{\partial z} \tag{1}$$

$$E_z = \frac{-j}{\omega\epsilon_r\epsilon_0}\frac{\partial H_y}{\partial x} \tag{2}$$

where ϵ_r is the relative permittivity. According to Floquet's theorem, electromagnetic fields in the periodic structure can be represented in terms of space harmonics whose phase constants in the z direction are

$$\beta_n = \beta + \frac{2\pi}{L}n, \qquad n = 0, \pm 1, \pm 2, \cdots \tag{3}$$

where β is the phase constant of the dominant space harmonic. The H_y component in the air, film, and substrate is given by

$$H_y(x,z) = \begin{cases} \sum_{n=-\infty}^{\infty} \tilde{A}_n e^{-\hat{w}_n(x-a)} e^{-j\beta_n z}, & a \leqslant x \\ \sum_{n=-\infty}^{\infty} \left(\tilde{B}_n \cos u_n x + \tilde{C}_n \sin u_n x\right) e^{-j\beta_n z}, & -a \leqslant x \leqslant a \\ \sum_{n=-\infty}^{\infty} \tilde{D}_n e^{w_n(x+a)} e^{-j\beta_n z}, & x \leqslant -a \end{cases} \tag{4}$$

where $\tilde{A}_n$, $\tilde{B}_n$, $\tilde{C}_n$, and $\tilde{D}_n$ are unknown expansion coefficients and $\hat{w}_n$, ju_n, and w_n are transverse propagation constants of the nth space harmonic in the air, film, and substrate, respectively. These parameters are related through the wave equation as

$$\hat{w}_n^2 = \beta_n^2 - k^2 \tag{5}$$

$$u_n^2 = \epsilon_{r2}k^2 - \beta_n^2 \tag{6}$$

$$w_n^2 = \beta_n^2 - \epsilon_{r3}k^2 \tag{7}$$

where k is the free space wavenumber and ϵ_{r2} and ϵ_{r3} are relative permittivities in the film and substrate, respectively.

The unknown phase constant β and expansion coefficients $\tilde{A}_n$, $\tilde{B}_n$, $\tilde{C}_n$, and $\tilde{D}_n$ are determined by matching the tangential electric and magnetic fields at $x=a$ and $x=-a$. The boundary conditions at the two interfaces are given by

$$H_{y2}(-a,z) = H_{y3}(-a,z) \tag{8}$$

$$E_{z2}(-a,z) = E_{z3}(-a,z) \tag{9}$$

$$H_{y2}(a,z) - H_{y1}(a,z) = J_z(z) = \begin{cases} I_z(z), & \text{on metallic strips} \\ 0, & \text{otherwise} \end{cases} \tag{10}$$

$$E_{z2}(a,z) = E_{z1}(a,z) \tag{11a}$$

$$E_{z2}(a,z) = E_{z1}(a,z) = 0, \qquad \text{on metallic strips} \tag{11b}$$

where the subscripts 1, 2, and 3 correspond to the cover, film, and substrate, respectively. $I_z(z)$ is the unknown surface current density in the z direction on the metallic strip. From (8)–(11a), expansion coefficients $\tilde{A}_n$, $\tilde{B}_n$, $\tilde{C}_n$, and $\tilde{D}_n$ are represented in terms of space harmonics of the surface current density $J_z(z)$ as

$$\tilde{A}_n = \left(\frac{1}{\epsilon_{r2}}\cdot\frac{u_n}{\hat{w}_n}\sin 2u_n a - \frac{1}{\epsilon_{r3}}\cdot\frac{w_n}{\hat{w}_n}\cos 2u_n a\right)\tilde{D}_n \tag{12a}$$

$$\tilde{B}_n = \left(\cos u_n a + \frac{\epsilon_{r2}}{\epsilon_{r3}}\cdot\frac{w_n}{u_n}\sin u_n a\right)\tilde{D}_n \tag{12b}$$

$$\tilde{C}_n = \left(-\sin u_n a + \frac{\epsilon_{r2}}{\epsilon_{r3}}\cdot\frac{w_n}{u_n}\cos u_n a\right)\tilde{D}_n \tag{12c}$$

$$\tilde{D}_n = \frac{1}{\left(1+\frac{1}{\epsilon_{r3}}\cdot\frac{w_n}{\hat{w}_n}\right)\cos 2u_n a + \left(\frac{\epsilon_{r2}}{\epsilon_{r3}}\cdot\frac{w_n}{u_n} - \frac{1}{\epsilon_{r2}}\cdot\frac{u_n}{\hat{w}_n}\right)\sin 2u_n a}\tilde{J}_{z,n} \tag{12d}$$

where

$$\tilde{J}_{z,n} = \frac{1}{L}\int_0^L J_z(z)e^{j\beta_n z}dz = \frac{1}{L}\int_0^{\delta} I_z(z)e^{j\beta_n z}dz. \tag{13}$$

Note that expansion coefficients $\tilde{A}_n$, $\tilde{B}_n$, $\tilde{C}_n$, and $\tilde{D}_n$ are as yet unknown, since the surface current density $J_z(z)$ is unknown, and $E_{z1}(a,z)$ and $E_{z2}(a,z)$ are not zero on the metallic strips, though they are continuous.

Before considering the remaining condition (11b), we expand the unknown $J_z(z)$ in terms of known basis functions $J_{z,m}(z)$ as

$$J_z(z) = \sum_{m=1}^{M} \alpha_m J_{z,m}(z) \tag{14}$$

where α_m is the unknown constant. The basis function $J_{z,m}(z)$ must be chosen so that it may be nonzero only on the metallic strips.

Now, we derive the eigenvalue equation by the imposition of the condition (11b). From (2), (4), (12a), (12d), and (14), $E_{z1}(a, z)$ is given by

$$E_{z1}(a,z)=\sum_{n=-\infty}^{\infty}\frac{j}{\omega\epsilon_0}\left\{\hat{w}_n\frac{\left(\frac{1}{\epsilon_{r2}}\cdot\frac{u_n}{\hat{w}_n}\sin 2u_na-\frac{1}{\epsilon_{r3}}\cdot\frac{w_n}{\hat{w}_n}\cos 2u_na\right)\sum_{m=1}^{M}\alpha_m\tilde{J}_{z,m,n}}{\left(1+\frac{1}{\epsilon_{r3}}\cdot\frac{w_n}{\hat{w}_n}\right)\cos 2u_na+\left(\frac{\epsilon_{r2}}{\epsilon_{r3}}\cdot\frac{w_n}{u_n}-\frac{1}{\epsilon_{r2}}\cdot\frac{u_n}{\hat{w}_n}\right)\sin 2u_na}\right\}e^{-j\beta_nz}\equiv\sum_{n=-\infty}^{\infty}\tilde{E}_ne^{-j\beta_nz} \quad (15)$$

where $\tilde{J}_{z,m,n}$ and $\tilde{E}_n$ are amplitude coefficients of the nth space harmonic of $J_{z,m}(z)$ and $E_{z1}(a, z)$, respectively. We multiply $\tilde{E}_n$ by $\tilde{J}^*_{z,s,n}$ for different values of s and sum over all n. This yields the following matrix equation:

$$\sum_{n=-\infty}^{\infty}\tilde{E}_n\tilde{J}^*_{z,s,n}=\sum_{m=1}^{M}\left\{\sum_{n=-\infty}^{\infty}\frac{j}{\omega\epsilon_0}\hat{w}_n\frac{\left(\frac{1}{\epsilon_{r2}}\cdot\frac{u_n}{\hat{w}_n}\sin 2u_na-\frac{1}{\epsilon_{r3}}\cdot\frac{w_n}{\hat{w}_n}\cos 2u_na\right)}{\left(1+\frac{1}{\epsilon_{r3}}\cdot\frac{w_n}{\hat{w}_n}\right)\cos 2u_na+\left(\frac{\epsilon_{r2}}{\epsilon_{r3}}\cdot\frac{w_n}{u_n}-\frac{1}{\epsilon_{r2}}\cdot\frac{u_n}{\hat{w}_n}\right)\sin 2u_na}\right.$$

$$\left.\cdot\tilde{J}_{z,m,n}\tilde{J}^*_{z,s,n}\right\}\alpha_m=\frac{1}{L}\int_0^L E_{z1}(a,z)J^*_{z,s}(z)\,dz=0, \qquad s=1,2,\cdots,M. \quad (16)$$

The above integration over a unit cell becomes zero, because $E_{z1}(a, z)$ is zero on the metallic strip and $J_{z,s}(z)$ zero otherwise. A nontrivial solution for α_m $(m=1,2,\cdots,M)$ exists only if the following determinantal equation holds:

$$\begin{vmatrix} G_{11} & G_{12} & \cdots & G_{1M} \\ G_{21} & G_{22} & \cdots & G_{2M} \\ \vdots & \vdots & & \vdots \\ G_{M1} & G_{M2} & \cdots & G_{MM} \end{vmatrix}=0 \quad (17)$$

where

$$G_{ij}=\sum_{n=-\infty}^{\infty}\hat{w}_n\frac{\left(\frac{1}{\epsilon_{r2}}\cdot\frac{u_n}{\hat{w}_n}\sin 2u_na-\frac{1}{\epsilon_{r3}}\cdot\frac{w_n}{\hat{w}_n}\cos 2u_na\right)}{\left(1+\frac{1}{\epsilon_{r3}}\cdot\frac{w_n}{\hat{w}_n}\right)\cos 2u_na+\left(\frac{\epsilon_{r2}}{\epsilon_{r3}}\cdot\frac{w_n}{u_n}-\frac{1}{\epsilon_{r2}}\cdot\frac{u_n}{\hat{w}_n}\right)\sin 2u_na}\tilde{J}_{z,j,n}\tilde{J}^*_{z,i,n}. \quad (18)$$

This is the eigenvalue equation that determines the phase constant β of the dominant space harmonic. On the other hand, the corresponding element G_{ij} for TE modes is

$$G_{ij}=\sum_{n=-\infty}^{\infty}\frac{\left(\frac{w_n}{u_n}\sin 2u_na+\cos 2u_na\right)}{w_n\left\{\left(1+\frac{\hat{w}_n}{w_n}\right)\cos 2u_na+\left(\frac{\hat{w}_n}{u_n}-\frac{u_n}{w_n}\right)\sin 2u_na\right\}}\tilde{J}_{y,j,n}\tilde{J}^*_{y,i,n} \quad (19)$$

where $\tilde{J}_{y,i,n}$ is the amplitude coefficient of the nth space harmonic of the basis function $J_{y,i}(z)$ for representing the unknown surface current $J_y(z)$ in the y direction. The above derivation process for the eigenvalue equation is generally called Galerkin's method. Therefore, the eigenvalue equation (17) becomes stationary for the phase constant β.

On the other hand, the dual formulation can be also obtained by expanding the field at the interface $x=a$ in terms of basis functions. The spectral domain approach in [11] for the microstrip and slot line is applicable to the formulation. Whether it is advantageous to use the current density or field depends upon the normalized width δ/L of the metallic strips. The comparison of the two approaches has not been made at the present stage.

III. Numerical and Experimental Results

The dispersion relation is given by seeking the root of the eigenvalue equation (17) numerically. The accuracy of the solution of our analysis is influenced by the choice of basis functions. If the exact current distribution on the metallic strip is given, the solution becomes exact. In the present paper, the following forms have been chosen for $J_{z,m}(z)$

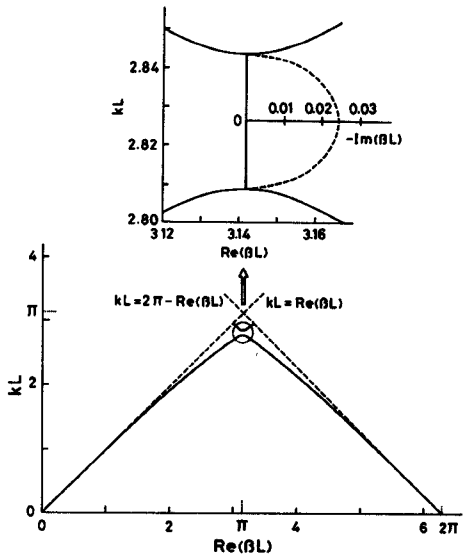

Fig. 2. Dispersion diagram for the lowest TM mode ($M=2$). $2a/L=0.5$, $\delta/L=0.25$, $\epsilon_{r2}=2.5$, $\epsilon_{r3}=1.0$.

TABLE I
CONVERGENCE OF $(kL)_c$, $\Delta(kL)/(kL)_c$, AND $-\mathrm{Im}(\beta L)_c$ AS THE NUMBER M OF BASIS FUNCTIONS INCREASES. $2a/L=0.5$, $\delta/L=0.25$, $\epsilon_{r2}=2.5$, $\epsilon_{r3}=1.0$

M	TE mode			TM mode		
	$(kL)_c$	$\frac{\Delta(kL)}{(kL)_c}$	$-\mathrm{Im}(\beta L)_c$	$(kL)_c$	$\frac{\Delta(kL)}{(kL)_c}$	$-\mathrm{Im}(\beta L)_c$
1	2.7475	0.1457	0.3689	2.8276	0.01130	0.02172
2	2.7500	0.1473	0.3758	2.8261	0.01233	0.02373
3	2.7508	0.1478	0.3779	2.8256	0.01268	0.02443
4	2.7511	0.1481	0.3790	2.8254	0.01286	0.02479

and $J_{y,m}(z)$

$$J_{z,m}(z)=\begin{cases}\sin\dfrac{(2m-1)\pi}{\delta}z, & 0\leqslant z\leqslant\delta \text{ for TM modes}\\ 0, & \delta\leqslant z\leqslant L \text{ for TM modes}\end{cases} \tag{20}$$

$$J_{y,m}(z)=\begin{cases}\cos\dfrac{2(m-1)\pi}{\delta}z, & 0\leqslant z\leqslant\delta \text{ for TE modes}\\ 0, & \delta\leqslant z\leqslant L \text{ for TE modes}\end{cases} \tag{21}$$

where δ is the width of the metallic strip. Although the current in the y direction tends to concentrate at the edges of the metallic strip, this effect is approximately taken into account.

Fig. 2 shows the typical dispersion diagram for the lowest TM mode. The enlarged dispersion diagram at the vicinity of a stopband is also shown in the inset in Fig. 2. As expected from the analogy of Bragg diffraction of X-rays in crystals, the stopband occurs at $\mathrm{Re}(\beta L)=\pi$. For frequencies in this region, β is complex. This stopband results from the coupling between the dominant space harmonic ($n=0$) of forward waves and the dominant space harmonic ($n=-1$) of backward waves. This phenomenon can be applied to band reject filters. In a forbidden region above the two lines $kL=\mathrm{Re}(\beta L)/\sqrt{\epsilon_{r3}}$ and $kL=2\pi-\mathrm{Re}(\beta L)/\sqrt{\epsilon_{r3}}$, the surface wave couples to a leaky wave that radiates outgoing beams. Here, consideration is given to the guiding rather than scattering properties.

Before presenting detailed guiding properties, we check the convergence of the solution of our analysis. Table I shows the convergence of the normalized center frequency $(kL)_c$ and width $\Delta(kL)/(kL)_c$ of the stopband, and the normalized attenuation constant $-\mathrm{Im}(\beta L)_c$ at the center frequency for different numbers of basis functions M. The normalized center frequency and width of the stopband are defined by

$$(kL)_c=[(kL)_u+(kL)_l]/2 \tag{22}$$

$$\frac{\Delta(kL)}{(kL)_c}=[(kL)_u-(kL)_l]/(kL)_c \tag{23}$$

where $(kL)_u$ and $(kL)_l$ are upper and lower stopband frequencies, respectively. It is found that even the approximation with $M=1$ provides good results. In the following numerical results, $M=2$ will be used.

Fig. 3 shows the normalized center frequency and width of the stopband, and the attenuation constant at the center frequency as a function of the width of the metallic strip. In Fig. 3(b), the results with $2a/L=1/3$ are not

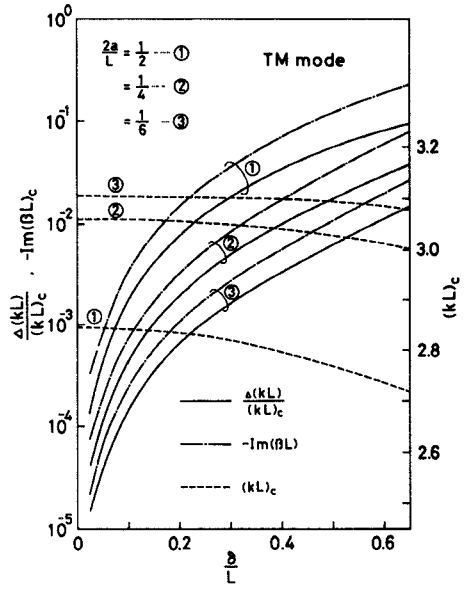

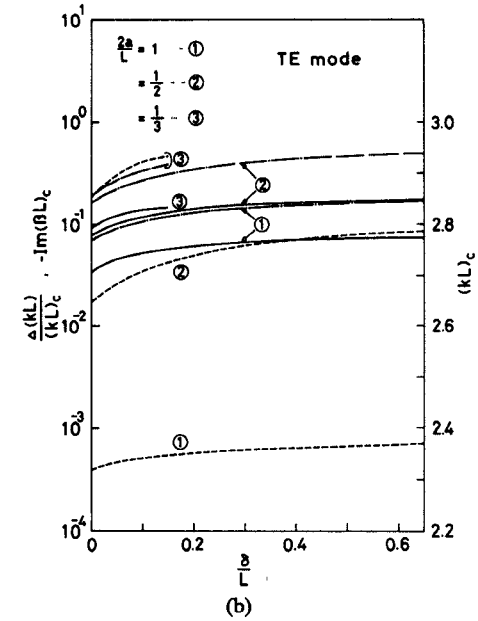

Fig. 3. Normalized center frequency and width of the stopband, and the normalized attenuation constant at the center frequency as a function of the width of the metallic strip. (a) TM mode. (b) TE mode. $\epsilon_{r2}=2.5$, $\epsilon_{r3}=1.0$.

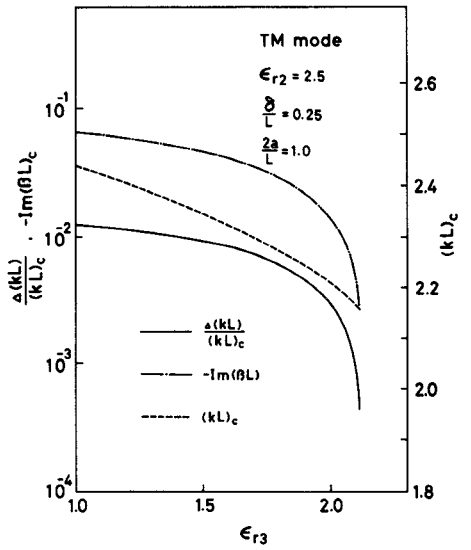

Fig. 4. Normalized center frequency and width of the stopband, and the normalized attenuation constant at the center frequency as a function of the relative permittivity ϵ_{r3} of the substrate.

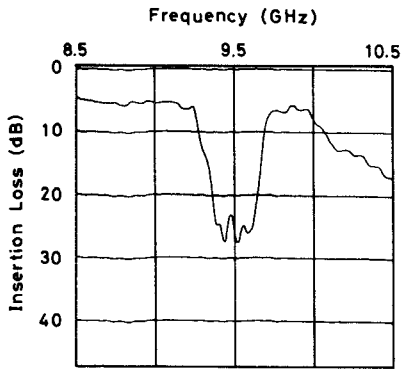

Fig. 5. Insertion loss for the TM mode of the band reject filter with the number of metallic strips = 40, $2a=8$ mm, $\delta=6$ mm, $L=14$ mm, $\epsilon_{r2}=2.25$, and $\epsilon_{r3}=1.0$.

shown for values of $\delta/L>0.15$, since the upper stopband frequency enters the forbidden region for that range. It is found that the width of the stopband and attenuation constant at the center frequency increase with the width of the metallic strip for both TM and TE modes. The center frequency of the stopband for the TM modes decreases with increasing δ/L in contrast to the case of TE modes. It is also found that the stopband properties for TE modes are not much influenced by the width of the strip, and the width of the stopband and the attenuation constant for TE modes are usually greater than those for TM modes. Moreover, there is a difference in the dependence of the stopband properties on $2a/L$ between TM and TE modes. The difference in the stopband properties of TM and TE modes has an important meaning for designing band reject filters.

Fig. 4 shows the normalized center frequency and width of the stopband, and the normalized attenuation constant at the center frequency as a function of relative permittivity ϵ_{r3} of the substrate. The width of the stopband becomes small as ϵ_{r3} approaches ϵ_{r2}, because the guiding region ($\sqrt{\epsilon_{r2}}>\mathrm{Re}(\beta/k)>\sqrt{\epsilon_{r3}}$) becomes small with decreasing $\epsilon_{r2}-\epsilon_{r3}$. In our example, the upper stopband frequency enters the forbidden region for values of $\epsilon_{r3}>2.11$.

In order to verify the validity of our analysis, experiments have been carried out at X-band. Band reject filters were fabricated by cementing metallic strips (aluminum) on the top of a polypropylene sheet ($\epsilon_r=2.25$). The surface wave was excited from a rectangular metallic waveguide using the flared horn. Fig. 5 shows the measured insertion loss of the band reject filter with the number of metallic

strips = 40, $2a = 8$ mm, $\delta = 6$ mm, and $L = 14$ mm. The width of the dielectric waveguide was 25 cm. The insertion loss of the dielectric waveguide without metallic strips was about 5 dB over a range of 8.5 to 10.5 GHz. The insertion loss includes the launching losses at the transmitting and receiving horns. The dielectric loss for the plane wave in the infinite polypropylene ($\tan\delta = 5 \times 10^{-4}$ [12]) is 0.58–0.72 dB/m over a range of measured frequencies, which approximates to the dielectric loss of the actual waveguide for the great field confinement. Therefore, most of the insertion loss is the launching loss. The transverse propagation constant in the y direction $k_y \simeq \pi/\text{width} = \pi/25[\text{cm}^{-1}]$ is considerably smaller than the wavenumber in the polypropylene $\sqrt{\epsilon_{r2}}\, k = 3\pi/\lambda$. Therefore, the fabricated filter approximates to the planar structure shown in Fig. 1. The calculated upper and lower stopband frequencies are 9.33 and 9.66 GHz, respectively, and the insertion loss at the center frequency of 9.50 GHz is 23.8 dB. The frequency where the dispersion curve enters into the forbidden region is 9.99 GHz. The increase of the insertion loss above the upper stopband frequency results from the coupling between the surface wave and the leaky wave. These experimental results agree with calculated values.

IV. Conclusion

A dielectric waveguide with periodic metallic strips suitable for millimeter-wave and submillimeter-wave integrated circuits has been investigated theoretically and experimentally. Stopband properties are numerically presented as a function of the spacing and width of metallic strips and dielectric profile. It is found that there is a difference in the stopband properties of TM and TE modes. For the fabrication of band reject filters, this difference should be taken into account. Experimental results for the band reject filter agree with theoretical values. The analysis presented in this paper can be applied to other types of periodic structures with metallic strips.

Acknowledgment

The author wishes to thank Prof. S. Nishida of Tohoku University for many helpful discussions and Prof. N. Okamoto of Shizuoka University for the loan of microwave instruments.

References

[1] K. Sakuda and A. Yariv, "Analysis of optical propagation in a corrugated dielectric waveguide," *Opt. Commun.*, vol. 8, no. 1, pp. 1–4, 1973.

[2] D. C. Flanders, H. Kogelnik, R. V. Schmidt, and C. V. Shank, "Grating filters for thin-film optical waveguides," *Appl. Phys. Lett.*, vol. 24, no. 4, pp. 194–196, 1974.

[3] M. L. Dakss, L. Kuhn, P. F. Heidrich, and B. A. Scott, "Grating coupler for efficient excitation of optical guided waves in thin films," *Appl. Phys. Lett.*, vol. 16, no. 12, pp. 523–525, 1970.

[4] K. Ogawa, W. S. C. Chang, B. L. Sopori, and F. J. Rosenbaum, "A theoretical analysis of etched grating couplers for integrated optics," *IEEE J. Quantum Electron.*, vol. QE-9, pp. 29–42, 1973.

[5] M. Nakamura, A. Yariv, H. W. Yen, S. Somekh, and H. L. Garvin, "Optically pumped GaAs surface laser with corrugation feedback," *Appl. Phys. Lett.*, vol. 22, no. 10, pp. 515–516, 1973.

[6] T. Itoh, "Application of gratings in a dielectric waveguide for leaky-wave antennas and band-reject filters," *IEEE Trans. Microwave Theory Tech.*, vol. MTT-25, pp. 1134–1138, 1977.

[7] R. C. Honey, "A flush-mounted leaky-wave antenna with predictable patterns," *IRE Trans. Antennas Propag.*, vol. AP-7, pp. 320–329, 1959.

[8] K. L. Klohn, R. E. Horn, H. Jacobs, and E. Freibergs, "Silicon waveguide frequency scanning linear array antenna," *IEEE Trans. Microwave Theory Tech.*, vol. MTT-26, pp. 764–773, 1978.

[9] C. H. Walter, *Traveling Wave Antennas*. New York: McGraw-Hill, 1965.

[10] T. Itoh and R. Mittra, "Dispersion characteristics of slot lines," *Electron. Lett.*, vol. 7, no. 13, pp. 364–365, 1971.

[11] J. B. Davies and D. Mirshekar-Syahkal, "Spectral domain solution of arbitrary coplanar transmission line with multilayer substrate," *IEEE Trans. Microwave Theory Tech.*, vol. MTT-25, pp. 143–146, 1977.

[12] J. F. Heitmann, "Theory and fabrication of dielectric image lines and measurements in the frequency range from 26.5 to 40 GHz," *Nachrichtentech. Z.*, vol. 28, pp. 279–284, 1975.